BOSTON UNIVERSITY

DEPARTMENT OF ELECTRICAL AND COMPUTER ENGINEERING

PhD Prospectus

DIRECTIONAL AND ENHANCED LIGHT EMISSION BASED ON PLASMONIC AND DIELECTRIC METASURFACES

By

XIAOWEI WANG
B.S., Huazhong University of Science and Technology, 2014
M.S., Boston University, 2016

Advisor: Prof. Roberto Paiella

ABSTRACT

Incoherent light sources, such as LEDs, emit light isotropically in all directions, but there are several applications where directional light emitters are of great importance, such as smart lighting, imaging, microdisplays, and optical wireless communications. Conventional optical components, such as lenses and waveplates, control the properties of the incident light by accumulating phase changes during propagation, which necessitates a propagation distance much longer than the optical wavelength. In this work, we investigate the unique properties of both plasmonic and dielectric metasurfaces, where subwavelength elements are applied to control the radiation properties of incoherent light emitters (colloidal quantum dots), to achieve the same functionality and at the same time enable strong emission-rate enhancements. These capabilities greatly favor the miniaturization and integration of optical devices, thus increasing device flexibility and potentially also decreasing production costs. Numerical simulation results and preliminary experimental data are presented in this prospectus, and the mechanisms behind their unique properties are explored.

1. INTRODUCTION

1.1 Motivation

Metasurfaces, which are artificially textured materials of subwavelength thickness, have received great attention in recent years [1-5]. They consist of specially designed planar nanoantenna arrays that can introduce any desired phase profile in their reflected or transmitted light. Compared to prior works based on metasurfaces, where the nanostructures are illuminated with externally incident light from a distant source [6-8], here we consider a different situation where the light-emitting sources are integrated on the metasurfaces, and explore ways to control their radiation properties in the near-field zone, favoring miniaturization and cost reduction.

In this thesis, we will first investigate the use of plasmonic gradient metasurfaces (GMSs) to produce directional light emission and strongly enhanced radiative rates. Then we will discuss the use of dielectric metasurfaces to increase the radiative efficiency of nearby active layers. Specifically, the coupling of Mie scattering resonances supported by high-index dielectric nanoparticles (NPs) and lattice surface modes (LSMs) will be explored. With much smaller absorption losses compared to metallic NPs, unparalleled energy efficiency could be obtained using dielectric metasurfaces. Finally, we will also show how the same systems could be utilized to produce directional beaming as well.

This document will begin by briefly covering some of the underlying theoretical concepts applied in this research.

1.2 Theoretical Background

a) Surface plasmon polaritons

Surface plasmon polaritons (SPPs) are electromagnetic surface waves propagating at the interface between a dielectric and a conductor. SPPs consist of coupled oscillations of the

conductor electron plasma at the surface ("surface plasmons") and electromagnetic waves in the adjacent dielectric medium. SPPs travel along and are evanescently confined to the metal-dielectric interface. The physical properties of SPPs can be investigated by solving Maxwell's equations at the interface.

We consider a simple one-dimensional problem at a single metal-dielectric interface, as defined in Fig. 1(a), where the propagation is only in the *x* direction and the permittivity ε only varies in the *z* direction. In the absence of external charge and current sources and assuming a time harmonic dependence of the electric fields, the Helmholtz wave equation is derived as $\nabla^2 \boldsymbol{E} + \varepsilon k_0^2 \boldsymbol{E} = 0$, where $k_0 = {}^{\omega}/_{c}$ is the wavenumber in vacuum. By matching the appropriate boundary conditions at the interface, we find that surface waves propagating along the interface only exist for transverse magnetic (TM) polarization and have the following dispersion relation:

$$k_x = \beta = k_o \sqrt{{}^{\varepsilon_1 \varepsilon_2}/_{\varepsilon_1 + \varepsilon_2}}\,, k_{z_{1,2}} = k_o \sqrt{{}^{\varepsilon_{1,2}^2}/_{\varepsilon_1 + \varepsilon_2}} \qquad (1)$$

where β is the propagation constant along *x* direction, and $k_{z_{1,2}}$ are the z components of the propagation constant in medium 1 and 2, respectively. Since β has to be real for propagation and $k_{z_{1,2}}$ have to be imaginary to ensure confinement in the *z* direction, we obtain the following constraints: $\varepsilon_1 \varepsilon_2 < 0$; $\varepsilon_1 + \varepsilon_2 < 0$, which are satisfied for metal-dielectric boundaries with frequencies below the bulk plasmon frequency ω_p.

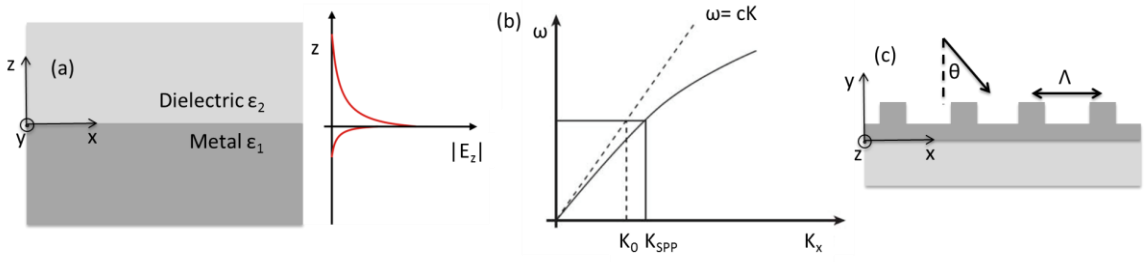

Fig. 1. (a) Geometry for SPP propagation at a single interface between a metal and a dielectric and plot of perpendicular electric field E_z. (b) Dispersion curves of light in dielectric layer (dashed line) and SPPs. (c) Plasmonic grating coupler.

The reciprocal of $|k_z|$ defines the evanescent decay length perpendicular to the interface. In the metal, the fields typically fall off over distances on the order of 20nm over a wide wavelength range. Hence, subwavelength metal structures can be utilized to support localized SPP resonances. By using the localized surface plasmons in metallic nanostructures, electromagnetic energy can be confined or squeezed into volumes smaller than the diffraction limit, leading to giant field enhancements [9-10]. On the other hand, β is greater than $\sqrt{\varepsilon_1} k_o$, which is the propagation constant of light in the isotropic, homogeneous dielectric layer, and therefore the SPP dispersion curve lies to the right of the dielectric light line, as shown in Fig. 1(b). As a result, it is impossible to directly couple to SPPs from radiating light unless some special techniques are employed to provide the required phase match. Different methods, such as prism coupling, have been

applied to overcome this momentum mismatch. Here we consider a simple example of a one-dimension grating, as depicted in Fig. 1(c).

In this geometry, the SPPs propagating along the surface and modulated by the gratings can couple to light and radiate (and vice versa). For light incident at an angle θ, the wave vector component along the surface is $k_x = k_0 \sin(\theta)$. The reciprocal lattice vector of the grating imparts the required additional momentum and thus coupling is allowed when the formula $\beta = k_x \mp q * {}^{2\pi}/_{\Lambda}$ is satisfied. Here q is an integer indicating the grating diffraction order and Λ is the grating period. By varying the grating period, the coupling of SPPs with light at different incident angles and/or different wavelengths is enabled.

When an ensemble of incoherent light emitters is located in the near-field vicinity of a metallic surface, a strong enhancement in emission rate can be produced through the direct excitation of SPPs. If these SPPs are excited on a flat dielectric/metal interface, eventually they get absorbed by ohmic dissipation in the metal, leading to a decrease in overall radiation intensity. In contrast, the coupling between a grating and SPPs can allow for efficient radiative scattering and therefore increased output light intensity.

b) Gradient metasurfaces

Metasurfaces are artificially textured surfaces composed of periodic subwavelength metal/dielectric nanostructures whose electric and/or magnetic response to the incident light is different from that of naturally occurring materials. Metasurfaces reduce the need for large propagation lengths with the ability to control radiation by abruptly changing the phase over distances much shorter than the wavelength.

GMSs are a specific type of metasurfaces that consist of a planar array of optical nanoantennas with specially designed shapes and dimensions to introduce a spatially linear phase shift in the light reflected or transmitted through the array [1-2, 6-8]. For GMSs with linearly position-dependent reflection phase $\psi(x) = \psi_0 + \xi\hat{x}$ along *x*, an incident wave with in-plane wave vector along the *x* direction k_x is scattered into a reflected beam having in-plane wave vector $k_x + \xi$, where ξ is the magnitude of the phase gradient [8]. Since any phase shift $\psi + n2\pi$ is the same as the phase shift ψ, folding the linear phase profile into a triangular one, this arrangement is equivalent to a blazed diffraction grating, where a sawtooth profile is utilized to produce one diffraction order with maximum diffraction efficiency [11]. GMSs therefore behave like blazed diffraction gratings, but with the distinct advantages of ultrathin flat geometry and simple fabrication involving only planar processing steps.

In a recent study [12], the radiation properties of an arbitrary light source located in the near field of a GMS with linear phase gradient were investigated. A homogenized continuum model (HCM) was applied to study the most general situation of a reflective GMS regardless of its specific design. In the HCM, the GMS is modeled as a perfect electric conductor (PEC) coated with a subwavelength metamaterial slab with a linearly position-dependent permittivity ε and permeability μ along *x* direction [Fig. 2], resulting in a linearly position-dependent reflection phase shift $\psi(x) = \psi_0 + \xi\hat{x}$. In this geometry, light emission is dominated by the excitation of evanescent surface waves, which are then diffracted by the GMS into radiation. Asymmetric directional radiation patterns

depending on the phase gradient $\xi$with greatly increased spontaneous emission rate were obtained. The GMS can also enhance the emission rate of dipole sources with internal quantum efficiency (IQE) less than about 10%. Due to the additional optical losses introduced by metallic nanostructures, however, the output power of dipole sources with higher IQE can be expected to be reduced.

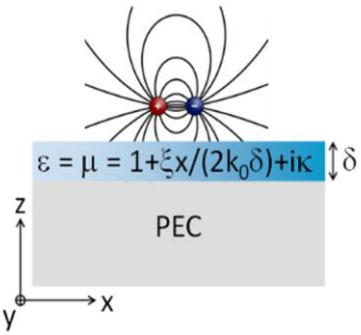

Fig. 2. Schematic cross-sectional view of the HCM model system used in the work of [12].

c) Dielectric nanoparticles

While plasmonic nanostructures are promising as a platform to concentrate light beyond the diffraction limit, they suffer from large optical losses in metals. This is the main factor hindering further enhancements of emission efficiency in some key applications. High-index dielectric NPs based on Mie scattering resonances are gaining great interest as an alternative to plasmonic systems due to their negligible absorption losses [13-18].

By Mie theory, when a high-index spherical NP is illuminated by a plane wave, electric-dipole and magnetic-dipole resonances (EDR and MDR) with comparable strengths can be generated. In particular, the incident light can excite circular displacement currents of the electric field inside the NP, leading to a magnetic Mie resonance when the wavelength is comparable to the NP diameter [14]. In this resonance, the electric field is concentrated at opposite sides of the particle with antiparallel orientation, while the magnetic field is maximum at the center. EDRs have the opposite field distributions. These optically induced electric dipoles are similar to the fundamental electric resonances of metallic NPs, but generally feature smaller field enhancements. In metallic particles, MDRs do not exist unless complex geometries are utilized, such as split-ring resonators similar to an effective inductor-capacitor circuit.

1.3 State-of-art

There have been other techniques explored for the directional beaming of luminescence, such as applying plasmonic gratings and photonic crystals, and near-field excitation of nanoscale antennas (e.g., with molecules and single quantum dots) [18-23]. However, the high precision required for aligning emitters to single nanoantennas and the inability to produce truly non-symmetric radiation patterns with plasmonic and photonic crystals can severely limit these approaches for device applications. In contrast, the GMS technique presented here solves both issues, since it is geared towards extended-area light

emitters (thus reducing the alignment precision requirement) and at the same time enables the realization of truly unidirectional emission control (by completely eliminating all diffraction orders except for one).

Plasmon-enhanced light emission has also been extensively studied in prior work [24-27]. As already discussed, plasmonic excitations can produce extremely high local-field intensities at the expense of additional optical losses. Although no such limitation applies to high-index dielectric NPs, their local-field enhancements are generally weaker and their scattering cross sections are smaller. In dielectric metasurfaces, by reducing the symmetry of the NPs, e.g., using nanodisks instead of spheres, the spectral positions of both EDR and MDR can be tuned by changing the aspect ratio. In a recent study [16], a moderate emission enhancement from quantum dots over a broad spectral band was obtained by overlapping these two resonances. In this work, we will study the coherent superposition of Mie resonances with LSMs, and show that the resulting excitations can provide an optimal tradeoff between the requirements of high local-field intensities and low optical losses for light-emission efficiency enhancement.

2. CURRENT WORK

2.1 Gradient-metasurface-enhanced light emission

a) Metasurface design

To obtain the linear position-dependent reflection phase, here we designed a one-dimensional GMS based on the procedure outlined in ref 10. It consists of a periodic array of *y*-oriented rectangular Au NPs supported by an optically thick Au film with a subwavelength SiO_2 spacer, as shown in Fig. 3(a) and the inset of Fig. 3(b). When a dipole emits light in the near field of this GMS, there will be electric currents generated in the Au NPs and in the reflection layer. Since these two metallic structures are very close to each other, strong near-field coupling will occur and generate a magnetic resonance [8-9]. The reflection phase is determined by the shape and dimensions of the Au NPs. When the NPs can be regarded as infinitely long in the *y* direction and the height in the *z* direction is fixed, the phase can be tuned by varying the NP width L_x. As shown by the FDTD simulation results of Fig. 3(b), the NP reflection phase (for *x*-polarized incident light at $\lambda_0 = 800$ nm) covers a large fraction of the entire 2π phase space, while at the same time a relatively high reflection amplitude > 83% is obtained for all values of L_x. The triangles and circles in Fig. 3(b) indicate, respectively, a set of three and four NP widths that produce equally spaced reflection-phase values across the full 2π range. The desired linear phase profile with gradient $\xi = 2\pi/\Lambda$ is then implemented with the periodic repetition of two alternating unit cells of length Λ, where each cell contains the (three or four) NPs from either set placed at equal distance ($\Lambda/3$ or $\Lambda/4$) from one another. A NP of zero width is included in both unit cells for fabrication convenience. The combined use of two different unit cells increases the number of forbidden diffraction orders for the resulting GMS (in the present design, all orders from $q = -10$ to $q = +11$ are suppressed except for the desired $q = +1$ order).

Figures 3(c)-(e) show the FDTD far-field radiation patterns produced by an *x*-, *y*- and *z*-oriented dipole source, respectively, located at the position denoted by the red dot in Fig. 3(a). The SPPs excited by the near-field interactions and then scattered into diffraction of order q = +1 by the GMS dominate the light emission process. Such diffractive scattering is most efficient for SPPs propagating along the *x*-direction (i.e., the direction of the phase gradient). As a result, for the *x*-polarized dipole (which predominantly excites SPPs along the *x* direction) the radiation pattern is peaked around the direction of in-plane wave vector $(-k_{SPP}+\xi)\hat{\mathbf{x}}$, where k_{SPP} is the SPP wavenumber. For Λ = 1000 nm and λ_0 = 800 nm, as in Fig. 3(c), the corresponding angles of peak emission are $\theta_{max} = \text{asin}((-k_{SPP}+\xi)/k_0) \approx 15°$ and $\varphi_{max} = 180°$. Similar considerations apply to the z-oriented dipole (which excites SPPs propagating in all directions isotropically), with a broader range of emitted azimuthal angles. Vice versa, the *y*-oriented dipole (which predominantly excites SPPs along the y direction) emits a more complex radiation pattern peaked near $\varphi_{max} = \pm 90°$, but with significantly lower intensity so that *x*-polarized emission is generally favored.

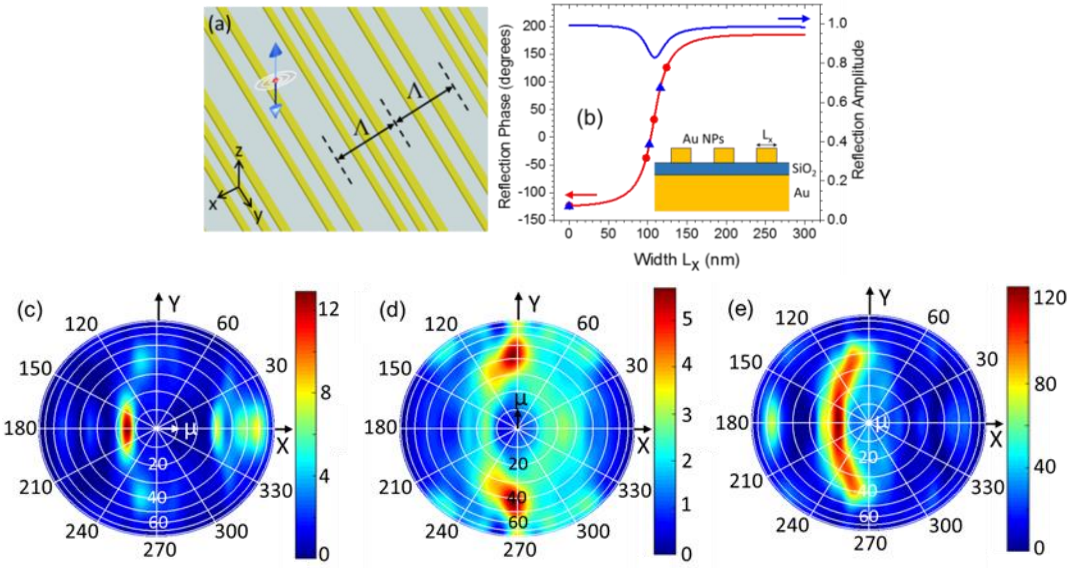

Fig. 3. (a) Reflective GMS design for directional light emission. (b) Calculated reflection phase (red trace) and amplitude (blue trace) of the nondiffractive periodic array of rectangular Au NPs shown in the inset, computed as a function of NP width L_x. (c)-(e) Calculated far-field radiation patterns of a dipole in the near-field zone of this GMS, with dipole moment $\boldsymbol{\mu}$ along the *x* ,*y* and *z*, respectively.

b) Experimental results

Experimental samples based on this GMS design were fabricated on a Si substrate using electron-beam lithography [as shown by the SEM image in Fig. 4(a)]. The samples are then planarized with a thin layer of spin-coated PMMA. CdTe/ZnS quantum dots (QDs) are employed as the radiation sources, whose emission peak covers the spectral range between 600nm and 1000nm, close to the resonance of the Au NPs. The QDs are suspended in a toluene/PLMA solution and then deposited by spin-casting, leading to a

homogeneous distribution of randomly-oriented light emitters at a fixed distance of about 10 nm over the NPs.

Fourier microscopy is used to characterize these samples, as shown in Figs. 4(b)-(d), where the unpolarized, *x*-polarized, and *y*-polarized far-field radiation patterns are depicted. The key predictions described above are observed in these plots, including: (1) highly directional emission peaked about the target angles $\theta_{max} = 15°$ and $\varphi_{max} = 180°$; (2) predominantly *x*-polarized radiation output (by 90% in the direction of peak emission); and (3) maximum emission for the *y* component near $\varphi_{max} = \pm 90°$. A large directivity D = 14 (8) is obtained from the *x*-polarized (unpolarized) pattern, with a very small divergence angle of 9° (11°) FWHM for the main beam in the line cut along the *x* direction [bottom plots of Figs. 4(b)-(c)]. The residual emission peak observed near $\theta = 15°$ and $\varphi = 0°$ is mostly due to deviations of the experimental NP widths from their target values.

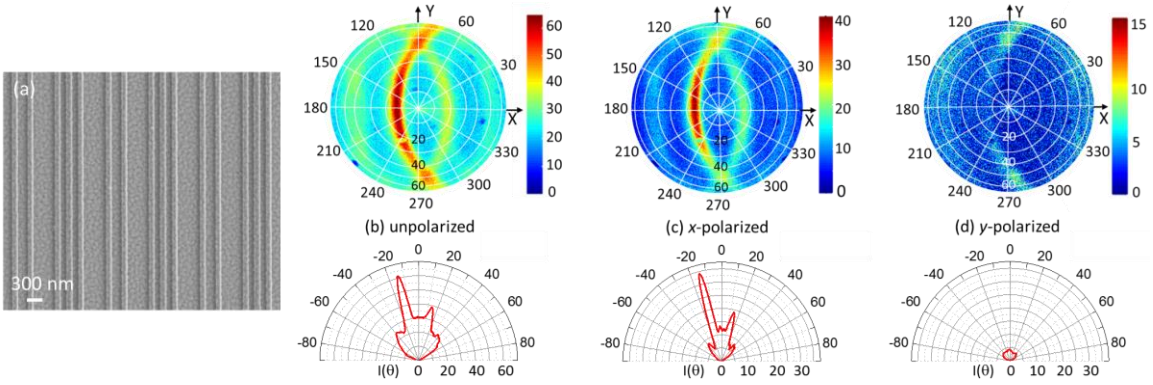

Fig. 4. (a) SEM image of a GMS based on the design of Fig. 3. (b)-(d) Unpolarized (b), *x*-polarized (c), and *y*-polarized (d) far-field radiation patterns of a similar GMS coated with CdTe/ZnS QDs. In each panel, the upper plot shows the full radiation pattern measured by Fourier microscopy, whereas the lower plot is a line cut along the *x*-axis. The PL signals are measured through a band pass filter centered at 800 nm.

2.2 Dielectric metasurfaces

Here we investigate numerically the constructive interference between LSMs and localized excitations of individual dielectric NPs. In planar periodic arrays of dielectric NPs with periods comparable to the EDR/MDR wavelengths, the diffractive scattering of incident light at the same wavelength produces a LSM propagating along the plane of the array. In turn, this surface wave can couple with the Mie resonances coherently, leading to a large additional increase in the near-field optical intensity. As a result, a new scattering resonance is produced featuring particularly narrow spectral lineshape and significantly increased average field intensities in the immediate vicinity of the NP array.

The specific metasurface geometry under study consists of a square-periodic array of Si nanocylinders supported by a SiO_2 substrate and embedded within a polymeric cap layer as shown in Fig. 5(a), with NP diameter *D* = 520 nm, height *H* = 170 nm, and

variable array period Λ. FDTD simulations were carried out to compute the local intensities of both electric and magnetic fields $|\mathbf{E}|^2$ and $|\mathbf{H}|^2$ in the immediate vicinity of the NPs, under illumination with a linearly polarized plane wave at normal incidence, normalized to the incident light. The resulting electric-field-intensity enhancement is finally averaged over the plane parallel to the array through the center of the NPs.

At sufficiently short periods [e.g., Λ = 700 nm in Fig. 5(b)], the spatially-averaged electric-field-intensity enhancement spectra, $\langle F_p \rangle$ versus λ_0, feature two pronounced peaks, corresponding to the NPs' fundamental MDRs and EDRs. This assignment is confirmed by the field-intensity enhancement maps shown in the figure insets. In the shorter-wavelength resonance, the magnetic field (mostly oriented along the *y* direction) displays a single intensity maximum inside each NP, which therefore behaves like a magnetic dipole. At the same time, the electric field circulates around the magnetic field, leading to a two-lobe intensity pattern on the monitor plane. The opposite behavior is observed at the longer resonance wavelength, consistent with the field distribution of an *x*-oriented electric dipole centered at each NP. A much smaller and narrower peak is also observed at a shorter wavelength, close to the array period multiplied by the refractive index of the cap layer (Λn_{cap} = 1042 nm), which indicates that this resonance is a LSM induced by first-order diffraction of the incident light.

As the array period Λ increases, all resonances are red shifted (at different rates) and eventually the LSM catches up with the MDR. As a result, the corresponding resonance peak in the field-intensity enhancement spectra is significantly increased and narrowed, as shown in Fig. 5(c). The hybrid nature of this excitation is illustrated by the maps shown in the insets. Inside each NP, the electric- and magnetic-field-intensity distributions exhibit a single node and antinode, respectively, consistent with MDR behavior. At the same time, nearly linear fringes oriented perpendicular to the *x* direction are also observed across the entire unit cell, suggesting a strong LSM contribution originating from the ($\pm$1, 0) diffraction of the incident light. Since oscillating magnetic and electric dipoles predominantly radiate in the direction perpendicular to their moment, the fringes orientation confirms the purely magnetic origin of such LSM. At even longer periods, the LSM is red shifted to overlap with the NPs EDR, and the opposite behavior is observed in the field-intensity maps, as shown in Fig. 5(d). Figure 5(e) shows the peak value of $\langle F_p \rangle$ for both electric and magnetic modes as a function of Λ: a remarkable increase in local field intensity is clearly produced by the coupling of these localized resonances with the array LSMs, up to a few 100s for the mixed LSM/MDR mode.

To illustrate the ability of such a dielectric metasurface to enhance light emission, we consider a continuous distribution of electric-dipole sources (e.g., colloidal QDs) on a monitor plane 10-nm above the NPs, whose emission rate is proportional to the average electric-field-intensity on the same plane. Figure 5(f) shows the radiative efficiency of this active layer η (and the ratio η/η_0) computed as a function of its IQE η_0, for emission at the mixed LSM/MDR wavelength of the metasurface of Fig. 5(c). Similar to the case of plasmon-enhanced light emission, large efficiency enhancements can be obtained for low values of η_0 (e.g., $\eta/\eta_0 > 100$ for $\eta_0 < 0.7\%$); at the same time, by virtue of their lossless nature, these dielectric systems can increase efficiency even in the high-η_0 limit,

where plasmonic NPs actually cause a degradation in output light intensity due to their large ohmic losses.

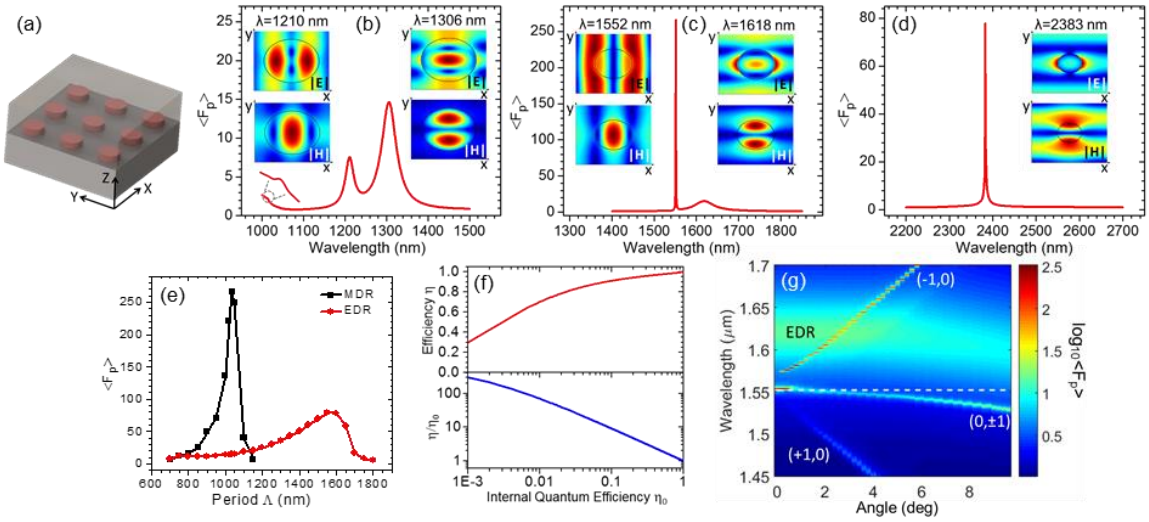

Fig. 5. (a) Schematic picture of the metasurfaces under study. (b)-(d) Spectra of the spatially-averaged electric-field-intensity enhancement $\langle F_p \rangle$ and field-intensity maps of the main resonances for three NP arrays with period Λ = 700 nm (b), 1035 nm (c), and 1600 nm (d). (e) $\langle F_p \rangle$ versus Λ for both electric and magnetic modes. (f) Radiative efficiency η (and ratio η/η_0) versus IQE η_0, for a distribution of dipole sources near the metasurface of (c) emitting at the mixed LSM/MDR wavelength. (g) Dispersion of $\langle F_p \rangle$ for the structure of (c).

Finally, the LSM/Mie resonances under study can also produce directional light emission from a nearby active layer, as a result of the diffractive nature of LSMs. This property is illustrated in the color map of Fig. 5(g), where $\langle F_p \rangle$ is plotted versus polar angle of incidence and wavelength, again for the design of Fig. 5(c). Due to the strong dispersion observed in this plot, if the emission wavelength is tuned to that of maximum field intensity at normal incidence (1552 nm, indicated by the dashed line), the dipole will primarily radiate in the direction perpendicular to the NP array. The same metasurface can therefore be used to enhance extraction (in addition to radiative) efficiency.

3. CONCLUSION

3.1 Summary

In this prospectus, directional and enhanced light emission based on plasmonic and dielectric metasurfaces has been proposed, designed and verified with FDTD simulations. The preliminary experimental results have been presented and the underlying theoretical concepts applied have also been discussed.

3.2 Future Work

i. *Design optimization:* New designs with more fabrication tolerance will be developed for the GMSs.

ii. *Fabrication and measurement of proposed devices*: GMSs with different angles of peak emission and dielectric metasurfaces will be fabricated and tested experimentally. Time-resolved photoluminescence spectroscopy will be used to measure the QD radiative lifetime, to demonstrate the expected large radiative-rate enhancements produced by the metasurfaces.

iii. *Further far-field beam shaping:* In this work so far, only the directional beaming capabilities of metasurfaces have been explored. However, there are other opportunities for engineering the far-field properties of the emitted light enabled by metasurfaces, including polarization control and the generation of more complex, nonlinear phase profiles, which will be further explored.

BIBLIOGRAPHY

1. Kildishev, Alexander V., Alexandra Boltasseva, and Vladimir M. Shalaev. "Planar photonics with metasurfaces." *Science* 339.6125 (2013): 1232009.

2. Yu, Nanfang, and Federico Capasso. "Flat optics with designer metasurfaces." *Nature materials* 13.2 (2014): 139.

3. Kuznetsov, Arseniy I., et al. "Optically resonant dielectric nanostructures." *Science* 354.6314 (2016): 2472.

4. Chen, Hou-Tong, Antoinette J. Taylor, and Nanfang Yu. "A review of metasurfaces: physics and applications." *Reports on Progress in Physics* 79.7 (2016): 076401.

5. Genevet, Patrice, et al. "Recent advances in planar optics: from plasmonic to dielectric metasurfaces." *Optica* 4.1 (2017): 139-152.

6. Sun, Shulin, et al. "Gradient-index meta-surfaces as a bridge linking propagating waves and surface waves." *Nature materials* 11.5 (2012): 426.

7. Sun, Shulin, et al. "High-efficiency broadband anomalous reflection by gradient meta-surfaces." *Nano letters* 12.12 (2012): 6223-6229.

8. Pors, Anders, et al. "Efficient unidirectional polarization-controlled excitation of surface plasmon polaritons." *Light: Science & Applications* 3.8 (2014): e197.

9. Maier, Stefan Alexander. Plasmonics: fundamentals and applications. *Springer Science & Business Media*, 2007.

10. Benson, Oliver. "Assembly of hybrid photonic architectures from nanophotonic constituents." *Nature* 480.7376 (2011): 193.

11. Larouche, Stéphane, and David R. Smith. "Reconciliation of generalized refraction with diffraction theory." *Optics letters* 37.12 (2012): 2391-2393.

12. Kogos, Leonard C., and Roberto Paiella. "Light emission near a gradient metasurface." *ACS Photonics* 3.2 (2016): 243-248.

13. Zhao, Qian, et al. "Mie resonance-based dielectric metamaterials." *Materials Today* 12.12 (2009): 60-69.

14. Kuznetsov, Arseniy I., et al. "Optically resonant dielectric nanostructures." *Science* 354.6314 (2016): 2472.

15. Kuznetsov, Arseniy I., et al. "Magnetic light." *Scientific reports* 2 (2012): 492.

16. Staude, Isabelle, et al. "Shaping photoluminescence spectra with magnetoelectric resonances in all-dielectric nanoparticles." *ACS Photonics* 2.2 (2015): 172-177.

17. Van de Groep, J., and A. Polman. "Designing dielectric resonators on substrates: Combining magnetic and electric resonances." *Optics express* 21.22 (2013): 26285-26302.

18. Staude, Isabelle, et al. "Tailoring directional scattering through magnetic and electric resonances in subwavelength silicon nanodisks." *ACS nano* 7.9 (2013): 7824-7832.

19. Lozano, G., et al. "Tailor-made directional emission in nanoimprinted plasmonic-based light-emitting devices." Nanoscale 6.15 (2014): 9223-9229.

20. Curto, Alberto G., et al. "Unidirectional emission of a quantum dot coupled to a nanoantenna." *Science* 329.5994 (2010): 930-933.

21. Aouani, Heykel, et al. "Bright unidirectional fluorescence emission of molecules in a nanoaperture with plasmonic corrugations." *Nano letters* 11.2 (2011): 637-644.

22. Lozano, Gabriel, et al. "Plasmonics for solid-state lighting: enhanced excitation and directional emission of highly efficient light sources." *Light: Science & Applications* 2.5 (2013): e66.

23. Giannini, V., G. Vecchi, and J. Gómez Rivas. "Lighting up multipolar surface plasmon polaritons by collective resonances in arrays of nanoantennas." *Physical review letters* 105.26 (2010): 266801.

24. Song, Jung-Hoon, et al. "Large enhancement of fluorescence efficiency from CdSe/ZnS quantum dots induced by resonant coupling to spatially controlled surface plasmons." *Nano letters* 5.8 (2005): 1557-1561.

25. Henson, John, et al. "Controlling the recombination rate of semiconductor active layers via coupling to dispersion-engineered surface plasmons." *JOSA B* 25.8 (2008): 1328-1335.

26. Henson, John, et al. "Plasmon-enhanced light emission based on lattice resonances of silver nanocylinder arrays." *Optics letters* 37.1 (2012): 79-81.

27. Paiella, Roberto. "Tunable surface plasmons in coupled metallo-dielectric multiple layers for light-emission efficiency enhancement." *Applied Physics Letters* 87.11 (2005): 111104.